II International Conference on Particle-based Methods - Fundamentals and Applications
PARTICLES 2011
E. Oñate and D.R.J. Owen (Eds)

QUASISTATIC GRANULAR MATERIAL RHEOLOGY FROM PARTICLE SIMULATIONS

J.-N. ROUX

Université Paris-Est, Laboratoire Navier, 2 Allée Kepler, Cité Descartes, 77420
Champs-sur-Marne, France.
E-mail: jean-noel.roux@ifsttar.fr

Key words: granular materials, elastoplasticity, stress-strain behaviour

Abstract. We report on the quasistatic behaviour of model granular materials, as probed by DEM simulations of isotropic compression and triaxial compression tests, focussing on the macroscopic behaviour dependence on control parameters expressed in dimensionless forms that combine contact laws with test conditions, and on the influence of the initial state. A discussion of the microscopic origins of strain, which in some situations of small strains and stable contact networks are due to contact deflections, and in other cases results from the continuous breaking and repairing of networks under varying loads provides a useful classification of rheological regimes. Some guidelines for parameter choices in numerical simulations, and for some homogenization approaches, are inferred.

1 INTRODUCTION

Discrete element simulations of granular systems have become a widespread approach, but its implementation requires adequate choices for many parameters. The mechanical properties of quasistatically deformed granular assemblies strongly depend on initial packing geometry. This communication is a contribution to the classification of initial states and quasistatic rheological regimes, based on simple state variables and dimensionless numbers, combining contact laws with externally imposed conditions. It addresses such issues as the sensitivity to contact stiffness and the rigid grain limit, the approach to the quasistatic limit and the effect of the initial coordination number, in addition to the initial density, on small to moderate strain response to deviator stresses (Sec. 3). First, Sec. 2 discusses possible states of isotropic packings and their response to isotropic compression. Sec. 4 lists a few remarkable conclusions.

2 MODEL MATERIAL AND SIMULATION PROCEDURE: ASSEMBLING STAGE AND COMPRESSION

We focus here on grain-level numerical simulations of the isotropic compression and the triaxial compression tests of assemblies of identical spherical beads, as in Refs. [1, 2, 3, 4]. Isotropic compression [5] is interesting both in itself and because it is a necessary preparation step, in simulations as well as in the laboratory, before a specimen is subjected to deviatoric loads and its internal shear resistance is probed.

2.1 Material definition, contact laws

We consider assemblies of N=4000 beads of diameter a, interacting at their contacts with (simplified) Hertz-Mindlin elasticity [6] and Coulomb friction, with coefficient μ (equal to 0.3, unless otherwise specified). Thus the normal elastic force F_N in contacts, assuming beads are made of an elastic material with Young modulus E and Poisson ratio ν, relates to the normal contact deflection, h, as $F_N = \frac{E\sqrt{a}}{1-\nu^2}h^{3/2}$ and the tangential force $\mathbf{F}_T$ varies incrementally with tangential relative displacement $\mathbf{u}_T$ at contacts as $d\mathbf{F}_T = K_T d\mathbf{u}_T$, involving stiffness parameter $K_T = \frac{2-2\nu}{2-\nu}\frac{dF_N}{dh}$, and subject to the Coulomb requirement $||\mathbf{F} - T|| \leq \mu F_N$. These relations should be supplemented by additional conditions ensuring thermodynamic consistence [7] and objectivity [8], as detailed in [3]. In order to damp out oscillations and accelerate the approach to mechanical equilibrium, some additional viscous forces in contacts might be introduced.

When a confining pressure P is applied, the deformation within grains in the contact regions is conveniently assessed by the *stiffness number* $\boxed{\kappa = \left[\frac{E}{(1-\nu^2)P}\right]^{2/3}}$ (contact deflections h are $\propto \kappa^{-1}$ [3]). For glass beads with $E = 70$ GPa and $\nu = 0.3$, the values used in the simulations reported in the sequel, one has $\kappa \simeq 8400$ for $P = 100$ kPa. Another important dimensionless control parameter is the *inertial number*, which is an indicator of the importance of dynamical effects in systems out of equilibrium. It is defined as $\boxed{I = \dot{\varepsilon}\sqrt{\frac{m}{aP}}}$ for grains of mass m when the macroscopic strain rate is $\dot{\varepsilon}$ [9, 2, 3, 10]. I is the ratio of inertial to deformation characteristic times. The quasistatic limit is simply defined as $I \to 0$.

It is convenient to implement fully periodic boundary conditions in all three directions and to perform partly stress-controlled tests. Stress components are evaluated in a specimen of volume Ω with the usual formula involving a sum over all contacts between pairs of particles i, j, where the contact force is $\mathbf{F}_{ij}$ and the branch vector $\mathbf{r}_{ij}$ points from the

Table 1: Isotropic states, with $\mu = 0.3$ ($\kappa \simeq 39000$ for A and C, $\kappa \simeq 181000$ for B and D), obtained with different assembling procedures.

Procedure	Φ	z^*	x_0 (%)
A ($\mu_0 = 0.$)	0.6370 ± 0.0002	6.074 ± 0.0015	1.3 ± 0.2
B ($\mu_0 = 0.02$)	0.6271 ± 0.0002	5.80 ± 0.007	1.95 ± 0.02
C (vibrated)	0.635 ± 0.002	4.56 ± 0.03	13.3 ± 0.5
D ($\mu_0 = \mu = 0.3$)	0.5923 ± 0.0006	4.546 ± 0.009	11.1 ± 0.4

center of i to the center of j, as

$$\sigma_{\alpha\beta} = \frac{1}{\Omega} \sum_{i<j} F_{ij}^{(\alpha)} r_{ij}^{(\beta)} \tag{1}$$

(if direct momentum transport due to particle velocities can be neglected). The dimensions of the simulation cell satisfy dynamical equations in order to impose prescribed values to some diagonal components of tensor $\underline{\underline{\sigma}}$ [3, 10, 11].

2.2 Initial states

In the assembling stage, a granular fluid is prepared at relatively low solid fraction (e.g., $\Phi = 0.45$, below hard sphere crystallization density $\Phi \simeq 0.49$) and randomized as a hard sphere (energy conserving) liquid, via an event-driven method. Then, an isotropic pressure is applied. In this first and all subsequent isotropic compressions, the system is requested to equilibrate under preset values of the applied pressure, with the condition that the strain rate should never exceed a certain threshold. In order to obtain different initial state densities and structures, one may use a different friction coefficient μ_0 in the initial sample preparation stage. Table 1 gives the basic characteristics of equilibrated packings built under low isotropic confining pressure (high κ): solid fraction Φ, fraction of "rattlers" (grains carrying no load) x_0, coordination number z^* of non-rattlers. A samples are built without friction ($\mu_0 = 0$), a well known procedure to obtain samples with the "random close packing" density [3], B ones are prepared with $\mu_0 = 0.02$, this small level of friction entailing a notable density change. D states are built with the final friction coefficient $\mu = 0.3$ acting in the granular gas stage ($\mu_0 = \mu = 0.3$), while compression is carried out slowly ($I \leq 10^{-3}$). Finally, C systems are assembled from A ones, after a slight dilation, strong vibrations, and recompaction to jamming with $\mu = 0.3$. Remarkably, they are nearly as dense as A ones, but with a low coordination number and a large population of rattlers.

2.3 Isotropic compression and pressure cycles

The results of the isotropic compression of the bead packs of Tab. 1 are shown in Fig. 1. The pressure dependence of solid fraction Φ in a compression cycle is nearly reversible (e.g., the initial small difference in density between A and C systems is retrieved), but the

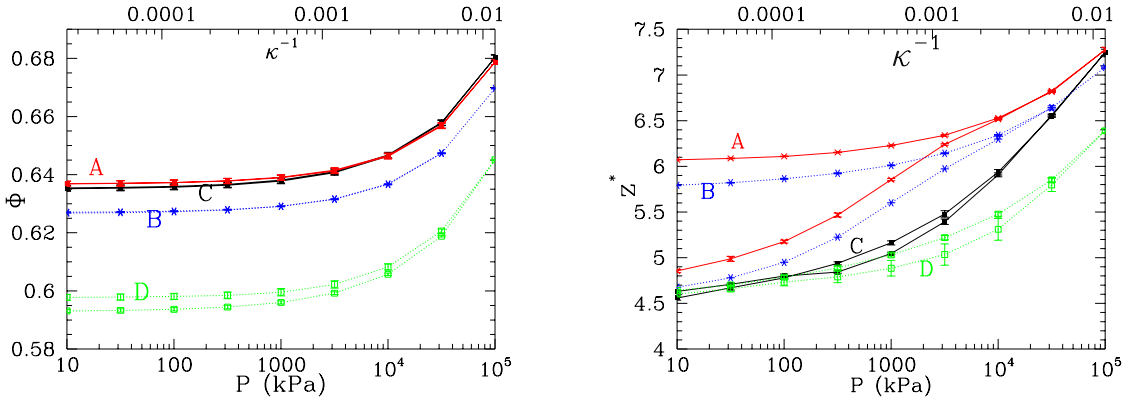

Figure 1: Effect of isotropic pressure cycle (from 10 to 10^4 kPa, and back down to 10 kPa) on samples of Tab. 1. Left: solid fraction Φ ; right: coordination number of non-rattlers, z^*.

internal structure might be strongly affected, as the initially high coordination number in systems A and B decreases upon unloading to low values (as in C and D).

2.4 Samples assembled with cohesion

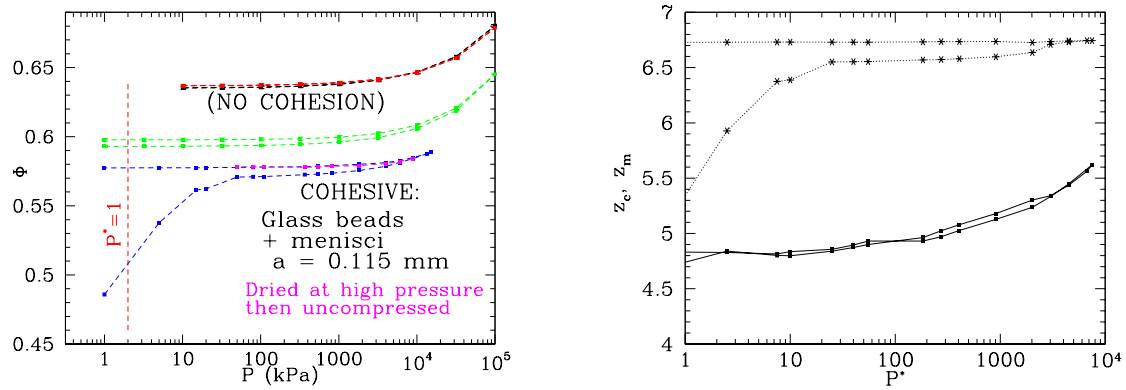

Figure 2: Effect of pressure cycle on system with capillary cohesion, similar to Fig. 1. Left: Φ (cohesionless results recalled for comparison) versus P; right: coordination number, of contacts z_c(bottom), of menisci, z_m (top), versus reduced pressure P^*.

In the presence of attractive forces in the contacts, much looser structures may be stabilized [12], provided the initially agitated particles of a granular gas are allowed to stick and form tenuous aggregates before the system is subjected to an external pressure. Fig. 2 displays a typical compression curve of an initially loose pack of beads with capillary cohesion, due to small menisci forming at intergranular contacts. Such an attractive force, with a meniscus of volume V joining two spheres of diameter a separated by distance D,

is conveniently approximated [13] as

$$F_c = F_0 \left[1 - \left(1 - \frac{4V}{\pi a D^2} \right)^{-1/2} \right], \quad \text{with} \quad F_0 = \pi \gamma a, \tag{2}$$

where γ is the surface tension and perfect wetting (zero contact angle) is assumed. These data correspond to volume $V = 10^{-3}a^3$ attributed to menisci that form when grains come into contact and break in receding pairs separated by distance $V^{1/3}$ [13]. The relative importance of cohesive forces and confining stress is expressed by dimensionless reduced pressure $\boxed{P^* = a^2 P/F_0}$ [12]: loose structures stabilized by attractive forces survive as long as P^* is small enough, and collapse as soon as the confining stress starts to dominate. The pressure cycle (Fig. 2) entails a large irreversible density increase, in which the contact coordination number hardly changes unless κ (Fig. 1) decreases too much. As cohesive forces become negligible under high P^*, they might be removed (as if wet grains were dried) with no effect on the subsequent density curve upon unloading (Fig. 2). The resulting cohesionless packing is looser than the loosest ones assembled with no cohesion (D in Tab. 1). Its coordination number and rattler density are similar to the values of states C or D of Table 1.

3 SIMULATIONS OF TRIAXIAL COMPRESSION

Triaxial compression testsare simulated with the standard procedure in which the *axial st rain rate* $\dot{\epsilon}_a$ is kept constant. The deviator stress, q, is measured, as a function of axial strain $\epsilon_a = \epsilon_1$, as $q = \sigma_1 - \sigma_3$, where σ_1 is the major ("axial") principal stress conjugate to ϵ_a, while the other two (lateral) principal stresses $\sigma_2 = \sigma_3$ are kept equal to the initial isotropic pressure P. The simulations reported here compare dense states A (high coordination number) and C (low coordination number). Pressure values, assuming particles are glass beads, vary between 10 kPa ($\kappa = 39000$) and 1 MPa ($\kappa = 1800$).

We first check for the approach of the quasistatic and the macroscopic limit in 3D, strain-rate controlled DEM simulations, then discuss the influence of coordination number, and sensitivity to stiffness parameter κ.

3.1 Reproducibility, quasistatic limit

Fig. 3 checks for stress-strain curve reproducibility in both A and C cases, for small axial strains. Thanks to the fully periodic boundary conditions [3], the macroscopic mechanical behavior is quite well defined with $N = 4000$. The approach to the quasistatic limit can be assessed on checking for the innocuousness of the dynamical parameters, i.e., inertial number I, and reduced damping parameter ζ. ζ is defined as the ratio of the viscous damping constant in a contact to its critical level, given the instantaneous value of the stiffness constant. We found it convenient to use a constant value of ζ in our simulations, as in [3]. Fig. 3 also shows that provided inertial number I, characterizing dynamical effects, is small enough, both I and ζ become irrelevant. Fig. 3 shows that the quasistatic

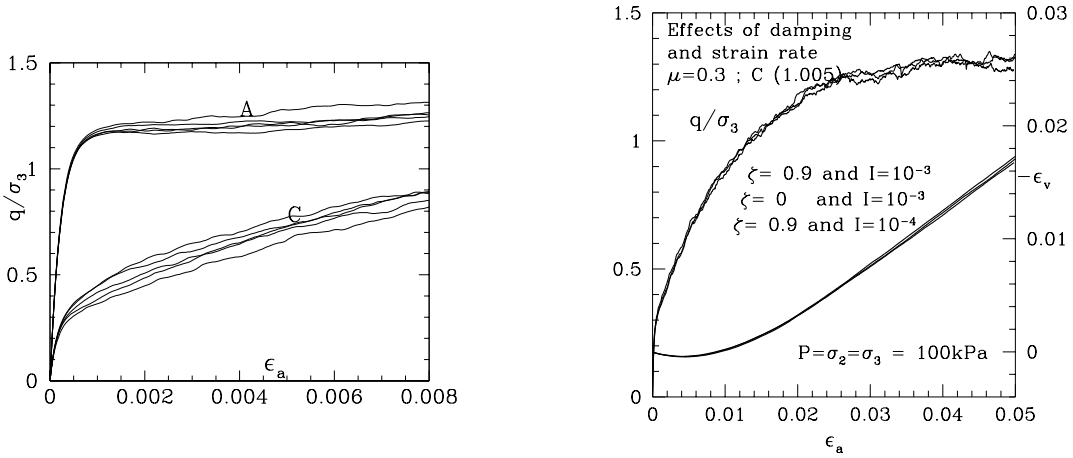

Figure 3: Left: small strain part of $q(\epsilon_a)$ curves for 5 different samples of each type, A (top curves) and C (bottom ones) with $N = 4000$ beads. Right: $q(\epsilon_a)$ and $\epsilon_v(\epsilon_a)$ curves in one type C sample for the different values of ζ and I indicated.

limit is correctly approached for $I \leq 10^{-3}$, quite a satisfactory result, given that usual laboratory tests with $\dot{\epsilon}_a \sim 10^{-5}$ s^{-1} correspond to $I \leq 10^{-8}$.

3.2 Influence of initial coordination number

Fig. 4 compares the behavior of initial states A and C, in triaxial compression with $P = 100$ kPa ($\kappa \simeq 8400$). Although, conforming to the traditional view that the peak

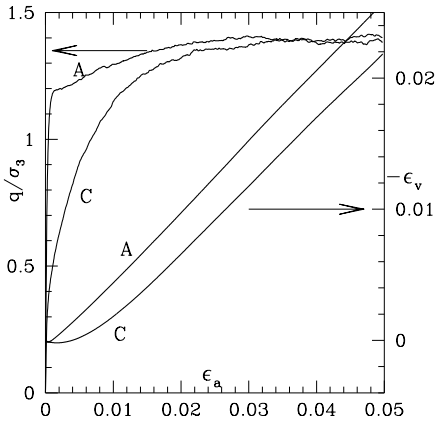

Figure 4: $q(\epsilon_a)$ (left scale) and $\epsilon_v(\epsilon_a)$ (right scale) curves for A and C states under $P = 100$ kPa. Averages over 5 samples of 4000 spherical grains.

deviator stress is determined by the initial sample density, maximum q values are very nearly identical in systems A and C, the mobilization of internal friction is much more gradual for C. For A, the initial rise of deviator q for small axial strain is quite steep, and

the volumetric strain variation becomes dilatant almost immediately, for $\epsilon_a \sim 10^{-3}$. In [4] it was shown that measurements of elastic moduli provide information on coordination numbers. It is thus conceivable to infer the rate of deviator increase as a function of axial strain from very small strain ($\sim 10^{-5}$ or below [14, 4]) elasticity. Most experimental curves obtained on sands, which do not exhibit q maxima or dilatancy before $\epsilon_a \sim 0.01$, are closer to C ones. However, some measurements on glass bead samples [15] do show fast rises of q at small strains, somewhat intermediate between numerical results of types A and C.

3.3 Influence of contact stiffness

The fast q increase in a small strain interval (say $\epsilon_a \leq 5.10^{-4}$) is sensitive to stiffness level κ. This is readily checked on changing the confining pressure. Fig. 5 shows the curves for triaxial compressions at different P values (separated by a factor $\sqrt{10}$) from 10 kPa to 1 MPa, with a rescaling of the strains by the stiffness parameter κ, in one A sample. They coincide for $q/P \leq 1$: within this wide deviator range, the macroscopic strain scales with contact deflections. This is clear evidence for a strain resulting from deformation at contacts – a regime we refer to as regime I (type I strains). For larger strains, curves

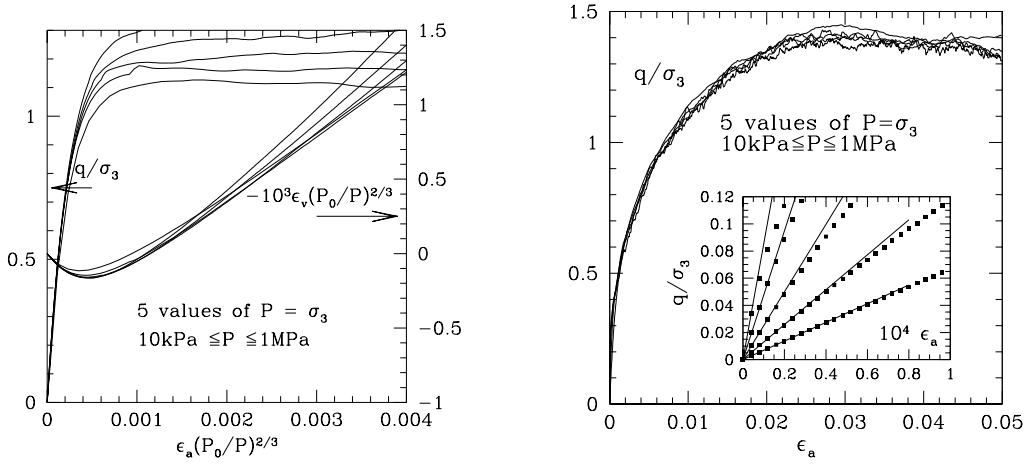

Figure 5: Left: $q(\epsilon_a)/P$ and $\epsilon_v(\epsilon_a)$ curves for one A sample and different P values. Strains on scale $(P/P_0)^{2/3} \propto \kappa^{-1}$, $P_0 = 100$ kPa. Right: $q(\epsilon_a)/P$ for the same P values in one C sample. Inset: detail with blown-up ϵ scale, straight lines corresponding to Young moduli in isotropic state.

separate on this scale, and tend to collapse together if q/P, ϵ_v are simply plotted versus ϵ_a. The strain dependence on stress ratio is independent from contact stiffness. This different sensitivity to pressure is characteristic of a rheological regime we refer to as regime II, in which strains are considerably larger and due to network rearrangement. Fig 5 also shows that it applies to C samples almost throughout the investigated range, down to small deviators (a behavior closer to most usual experimental results on sands than type A configurations). At the origin (close to the initial isotropic state, see inset on

fig. 5, right plot), the tangent to the curve is given by the elastic (Young) modulus of the granular material, E_m, and therefore q/P scales with κ, but curves quickly depart from this behaviour (around $q = 0.2P$). The approximately elastic range [4] is quite small, as observed in experiments [14, 16, 17].

As to the isotropic compression tests of Sec. 2, they are obviously in regime I in cohesionless systems, and in regime II for loose cohesive structures.

3.4 Calculations with a fixed contact list

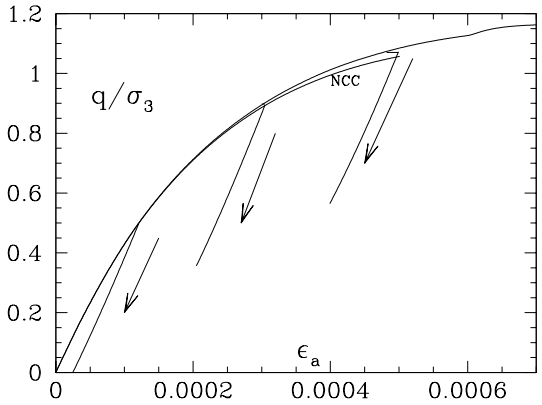

Figure 6: Very small strain part of $q(\epsilon_a)$ curve in one A sample, showing beginning of unloading curves (arrows). Curve marked NCC was obtained on calculating the evolution of the same sample without any contact creation.

Within regime I, the mechanical properties of the material can be successfully predicted on studying the response of one given set of contacts. Those might slide or open, but the very few new contacts that are created can be neglected. To check this in simulations, one may restrict at each time step the search for interacting grains to the list of initially contacting pairs. Fig. 6 compares such a procedure to the complete calculation. The curve marked "NCC" for *no contact creation* is indistinguishable from the other one for $q \geq 0.8$. We thus check that, in regime I, the macroscopic behavior is essentially determined by the response of a fixed contact network.

3.5 Type I strains and elastic reponse

Fig. 6 also shows that the small strain response of A samples, within regime I, close to the initial state, is already irreversible: type I strains are not elastic. An approximately elastic behavior is only observed for very small strains, as depicted in the inset of Fig. 5 (right graph). In this small interval near the initial equilibrium configuration, the stress-strain curve is close to its initial tangent, defined by the elastic modulus. Moduli [4] can be calculated from the stiffness matrix of contact networks. One may also check that the unloading curves shown on Fig. 6 comprise a small, approximately elastic part, with the relevant elastic modulus (the Young modulus for a triaxial test at constant lateral stress)

defining the initial slope. At the microscopic level, a small elastic response is retrieved upon reversing the loading direction because contacts stop sliding. The elastic range is strictly included in the larger range of type I behavior.

3.5.1 Fluctuations and length scale

Finally, let us note that regimes I and II also differ by the importance of sample to sample fluctuations: curves in Fig. 3 (left plot) pertaining to the different samples of type A or C are confused as long as $q \leq 1.1P$ (case A) or $q \leq 0.3P$ (case C), which roughly corresponds to the transition from regime I to regime II. Larger fluctuations imply that the characteristic length scale associated with the displacement field (correlation length) is larger in regime II. Whether and in what sense rearrangements triggered by instabilities in regime II, in a material close to the rigid limit (large κ), can be regarded as local events is still an open issue.

4 SOME CONCLUSIONS

This brief account of isotropic and triaxial tests on model material for different initial states reveals that the initial states should be classified according to their coordination number in addition to their density, as dense systems might be as poorly coordinated as loose ones. Compression test results are independent of dynamical parameters if the inertia parameter I is kept small enough. The response to an isotropic compression of cohesionless systems is apparently elastic as density changes are close to reversible, but contact networks exhibit irreversible changes in pressure cycles, with a very notable decrease in coordination number if its riginal value was large. Cohesion may stabilize loose structure that collapse under growing applied load, and density increase in compression then depend on the maximum value of reduced pressure P^* in the sample history, rather than on stiffness parameter κ. Regime I corresponds to the stability range of a given contact structure. It is larger in highly coordinated systems. It is observed in the beginning of monotonic loading tests, in which the deviator stress increases from an initial isotropic configuration, and also after changes in the direction of load increments (hence a loss in friction mobilization). Strains, for a given stress level, are then inversely proportional to contact stiffnesses. The deviator range in regime I, in usual monotonic tests, is stricly larger than the small elastic range, but strictly smaller than the maximum deviator. It was shown in previous studies of 2D systems [18, 19, 20] not to vanish in the limit of large systems, unlike in the singular case of rigid, frictionless particle assemblies [21, 22]. Regime I is limited by the occurrence of elastoplastic instabilities in the contact network and does not coincide with the prediction of the critical yield approach. In regime I, the work of the externally applied load is constantly balanced by the one of contact forces, so that the kinetic energy approaches zero in the limit of slow loading rates. A remarkable consequence is that the instability condition based on the negativity of the macroscopic second-order work [23] is never fulfilled, as macroscopic and microscopic works coincide,

and the latter is positive. In regime II, network rearrangements are triggered by instabilities and some bursts of kinetic energy are observed [24]. Larger fluctuations witness longer-ranged correlations in the displacements. The microscopic origin of macroscopic strains, which are independent on contact elasticity for usual stiffness levels κ, lies in the geometry of grain packings.

On attempting to predict a macroscopic mechanical response from packing geometry and contact laws, the information about which kind of strain should dominate is crucial.

REFERENCES

[1] A. S. J. Suiker and N. A. Fleck. Frictional collapse of granular assemblies. *ASME Journal of Applied Mechanics*, 71:350–358, 2004.

[2] J.-N. Roux. The nature of quasistatic deformation in granular materials. In R. García Rojo, H. J. Herrmann, and S. McNamara, editors, *Powders and Grains 2005*, pages 261–265, Leiden, 2005. Balkema.

[3] I. Agnolin and J.-N. Roux. Internal states of model isotropic granular packings. I. Assembling process, geometry, and contact networks. *Phys. Rev. E*, 76:061302, 2007.

[4] I. Agnolin and J.-N. Roux. Internal states of model isotropic granular packings. III. Elastic properties. *Phys. Rev. E*, 76:061304, 2007.

[5] I. Agnolin and J.-N. Roux. Internal states of model isotropic granular packings. II. Compression and pressure cycles. *Phys. Rev. E*, 76:061303, 2007.

[6] K. L. Johnson. *Contact Mechanics*. Cambridge University Press, 1985.

[7] D. Elata and J. G. Berryman. Contact force-displacement laws and the mechanical behavior of random packs of identical spheres. *Mechanics of Materials*, 24:229–240, 1996.

[8] M. R. Kuhn and C. S. Chang. Stability, Bifurcation and Softening in Discrete Systems: A Conceptual Approach for Granular Materials. *International Journal of Solids and Structures*, 43:6026–6051, 2006.

[9] GDR MiDi. On dense granular flows. *European Physical Journal E*, 14:341–365, 2004.

[10] P.-E. Peyneau and J.-N. Roux. Frictionless bead packs have macroscopic friction, but no dilatancy. *Phys. Rev. E*, 78:011307, 2008.

[11] F. Radjaï and C. Voivret. Periodic Boundary Conditions. In *Discrete-element Modeling of Granular Materials*.

[12] F. A. Gilabert, J.-N. Roux, and A. Castellanos. Computer simulation of model cohesive powders: Influence of assembling procedure and contact laws on low consolidation states. *Phys. Rev. E*, 75(1):011303, 2007.

[13] O. Pitois, P. Moucheront, and X. Chateau. Liquid bridge between two moving spheres: An experimental study of viscosity effects. *J. Coll. Interf. Sci.*, 231:26–31, 2000.

[14] S Shibuya, F. Tatsuoka, S. Teachavorasinskun, X.-J. Kong, F. Abe, Y.-S. Kim, and C.-S. Park. Elastic deformation properties of geomaterials. *Soils Found.*, 32:26–46, 1992.

[15] S. Emam, J. Canou, A. Corfdir, J.-C. Dupla, and J.-N. Roux. élaboration et comportement mécanique de matériaux granulaires solides modèles : expériences et simulations numériques. In B. Cazacliu and J.-N. Roux, editors, *Rhélogie des pâtes et des matériaux granulaires*, volume SI12 of *Etudes et Recherches des Laboratoires des Ponts et Chaussées*, pages 105–145, Paris, 2006. Presses du Laboratoire Central des Ponts et Chaussées.

[16] H. di Benedetto, H. Geoffroy, C. Sauzéat, and B. Cazacliu. Sand behaviour in very small to medium strain domains. In M. Jamiolkowski, R. Lancellotta, and D. Lo Presti, editors, *Pre-failure Deformation Characteristics of Geomaterials*, pages 89–96, Rotterdam, 1999. Balkema.

[17] R. Kuwano and R. J. Jardine. On the applicability of cross-anisotropic elasticity to granular materials at very small strains. *Géotechnique*, 52:727–749, 2002.

[18] G. Combe. *Mécanique des matériaux granulaires et origines microscopiques de la déformation*. Presses du Laboratoire Central des Ponts et Chaussées, Paris, 2002.

[19] J.-N. Roux and G. Combe. Quasistatic rheology and the origins of strain. *Comptes Rendus Physique*, 3:131–140, 2002.

[20] J.-N. Roux and G. Combe. How granular materials deform in quasistatic conditions. In J. D. Goddard, J. T. Jenkins, and P. Giovine, editors, *IUTAM-ISIMM symposium on mathematical modeling and physical instances of granular flow*, volume 1227 of *AIP conference proceedings*, pages 260–270. AIP, 2010.

[21] G. Combe and J.-N. Roux. Strain versus stress in a model granular material: a devil's staircase. *Phys. Rev. Lett.*, 85:3628–3631, 2000.

[22] P.-E. Peyneau and J.-N. Roux. Solidlike behavior and anisotropy in rigid frictionless beas assemblies. *Phys. Rev. E*, 78:041307, 2008.

[23] F. Prunier, F. Laoufa, and F. Darve. 3d bifurcation theory in geomaterials. Investigation of the second order work criterion. *European Journal of Environmental and Civil Engineering*, 13:135–147, 2009.

[24] L. Staron, J-P. Vilotte, and F. Radjaï. Pre-avalanche instabilities in a tilted granular pile. *Phys. Rev. Lett.*, 89:204302, 2002.